AIP | Applied Physics Letters

Schottky barrier contrasts in single and bi-layer graphene contacts for MoS2 field-effect transistors

Hyewon Du, Taekwang Kim, Somyeong Shin, Dahye Kim, Hakseong Kim, Ji Ho Sung, Myoung Jae Lee, David H. Seo, Sang Wook Lee, Moon-Ho Jo, and Sunae Seo

Citation: Applied Physics Letters **107**, 233106 (2015); doi: 10.1063/1.4937266
View online: http://dx.doi.org/10.1063/1.4937266
View Table of Contents: http://scitation.aip.org/content/aip/journal/apl/107/23?ver=pdfcov
Published by the AIP Publishing

Schottky barrier contrasts in single and bi-layer graphene contacts for MoS_2 field-effect transistors

Hyewon Du,[1] Taekwang Kim,[1] Somyeong Shin,[1] Dahye Kim,[1] Hakseong Kim,[2] Ji Ho Sung,[3,4] Myoung Jae Lee,[3] David H. Seo,[5] Sang Wook Lee,[2] Moon-Ho Jo,[3,4] and Sunae Seo[1,a)]

[1]*Department of Physics, Sejong University, Seoul 143-747, South Korea*
[2]*Divison of Quantum Phases and Devices, Department of Physics, Konkuk University, Seoul 143-701, South Korea*
[3]*Center for Artificial Low-Dimensional Electronic Systems, Institute for Basic Science (IBS), 77 Cheongam-Ro, Pohang 790-784, South Korea*
[4]*Division of Advanced Materials Science, Pohang University of Science and Technology (POSTECH), 77 Cheongam-Ro, Pohang 790-784, South Korea*
[5]*Samsung Electronics Company, Limited, System LSI Division, TD Team, Gyunggi 446-711, South Korea*

(Received 12 September 2015; accepted 9 November 2015; published online 8 December 2015)

We have investigated single- and bi-layer graphene as source-drain electrodes for n-type MoS_2 transistors. Ti-MoS_2-graphene heterojunction transistors using both single-layer MoS_2 (1M) and 4-layer MoS_2 (4M) were fabricated in order to compare graphene electrodes with commonly used Ti electrodes. MoS_2-graphene Schottky barrier provided electron injection efficiency up to 130 times higher in the subthreshold regime when compared with MoS_2-Ti, which resulted in V_{DS} polarity dependence of device parameters such as threshold voltage (V_{TH}) and subthreshold swing (SS). Comparing single-layer graphene (SG) with bi-layer graphene (BG) in 4M devices, SG electrodes exhibited enhanced device performance with higher on/off ratio and increased field-effect mobility (μ_{FE}) due to more sensitive Fermi level shift by gate voltage. Meanwhile, in the strongly accumulated regime, we observed opposing behavior depending on MoS_2 thickness for both SG and BG contacts. Differential conductance (σ_d) of 1M increases with V_{DS} irrespective of V_{DS} polarity, while σ_d of 4M ceases monotonic growth at positive V_{DS} values transitioning to ohmic-like contact formation. Nevertheless, the low absolute value of σ_d saturation of the 4M-graphene junction demonstrates that graphene electrode could be unfavorable for high current carrying transistors. [http://dx.doi.org/10.1063/1.4937266]

Previous in-depth studies on two-dimensional (2D) MoS_2 transistors have demonstrated excellent field-effect mobility with high on-off ratio at room temperature.[1–3] However, Schottky barrier (SB) formation[4] or wetting issues of metal-MoS_2 have limited device performance.[5] Even the most commonly studied MoS_2-Ti contact has been the subject of much debate regarding the formation of ohmic[2] or Schottky contacts.[1] Similar controversy exists for graphene-MoS_2 contacts.[6,7] Previously, improved MoS_2 device properties were reported by utilizing graphene rather than metal contacts which resulted in an unexpectedly lower SB height in comparison with MoS_2-metal junctions.[7,8] However, due to high sheet resistance of intrinsic monolayer graphene, doping or multi-layer graphene has been introduced.[9]

We fabricated three back-gated MoS_2 field-effect transistors (FETs) with Ti and graphene asymmetric electrodes in each device for direct comparisons in transistor performance. Three different FETs: single-layer MoS_2/single-layer graphene (1M-SG), 4-layer MoS_2/single-layer graphene (4M-SG), and 4-layer MoS_2/bi-layer graphene (4M-BG) were fabricated. The channel length/width (L/W) of each device was 2.6 μm/6.2 μm, 3.4 μm/3.2 μm, and 2.8 μm/5.5 μm for 1M-SG, 4M-SG, and 4M-BG, respectively. The characterization of thickness for MoS_2 and graphene including Raman spectrum and atomic force microscope imaging, as well as detailed transistor fabrication processes are described in the supplementary material.[10]

The transfer curves (I_{DS}-V_{BG}) and output curves (I_{DS}-V_{DS}) for our three devices are presented in Figs. 1(d)–1(f) and 1(g)–1(i), respectively, where I_{DS} is source-drain channel current and V_{BG} and V_{DS} are back gate voltage and source-drain voltage, respectively. V_{DS} is applied at the Ti electrode with grounded graphene electrode. All three devices demonstrate n-channel transistor behavior with on/off ratio of 10^6–10^7.

Nonlinear and asymmetric output characteristics in Figs. 1(j)–1(l) demonstrate back-to-back SB formation in fabricated MoS_2 transistors. Photocurrent data at $V_{BG} = 0$ V also support the existence of SBs.[10] In contrast to conventional Si transistors, output curves show non-linearity rather than initially linear regimes and subsequent saturation with the increase in V_{DS}.

4M devices (4M-SG and 4M-BG) show larger off (I_{OFF}) and on current (I_{ON}) than 1M device (1M-SG). The higher I_{DS} in 1M devices can be explained by a few factors. First, the band gap of MoS_2 shows a transition from indirect to direct gap with monotonic increase from 1.3 eV for bulk to 1.9 eV for single-layer, while electron affinity also diminishes from 4.4 eV to 3.7 eV.[11] Therefore, thickness decrease

a)Author to whom correspondence should be addressed. Electronic mail: sunaeseo@sejong.ac.kr

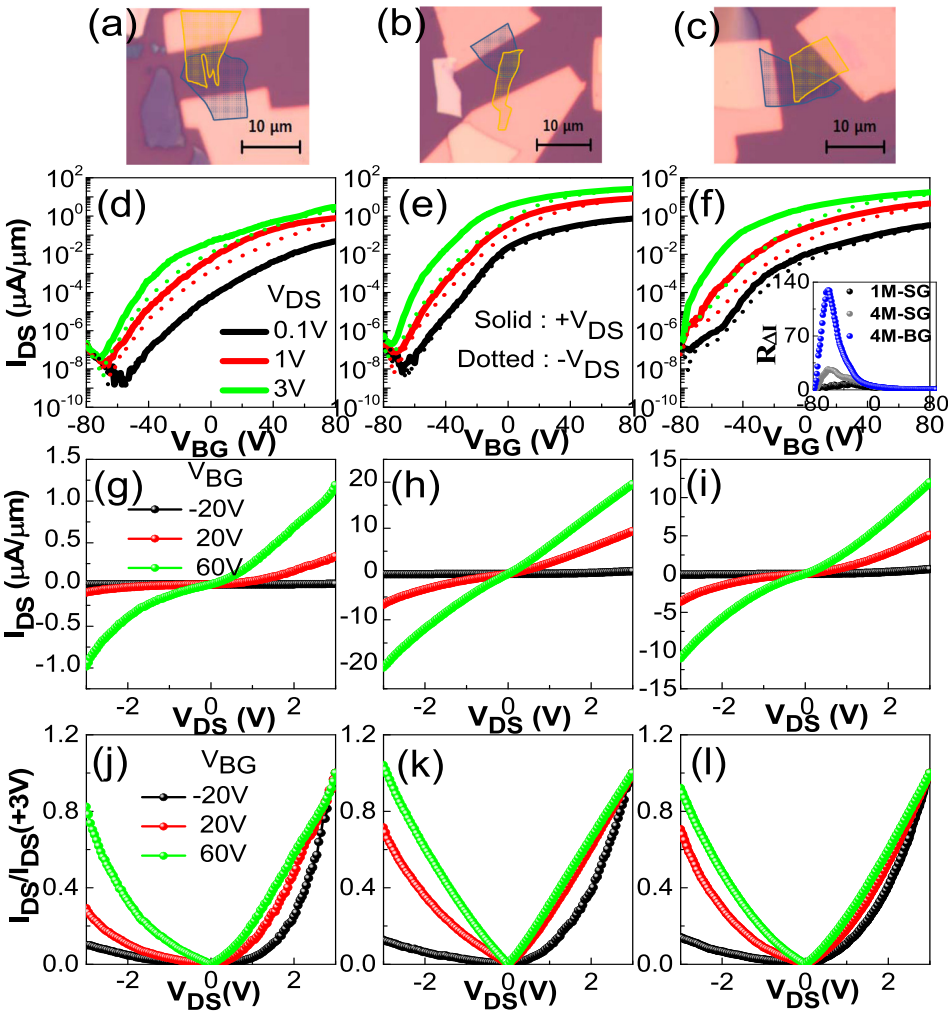

FIG. 1. (a)-(c) Optical images indicating MoS_2 area enclosed with yellow lines and graphene area enclosed with blue lines, (d)-(f) I_{DS}-V_{BG}, (g)-(i) I_{DS}-V_{DS}, and (j)-(l) I_{DS} normalized by I_{DS} at $V_{DS} = +3$ V. (a), (d), (g), and (j) for 1M-SG; (b), (e), (h), and (k) for 4M-SG; (c), (f), (i), and (l) for 4M-BG.

accompanies the decrease in intrinsic conductivity in MoS_2 and the increase in SB height in MoS_2-graphene junction. Second, the depth of the surface channel known to be 6–10 nm in 2D MoS_2[12] affects transport properties in both 1M and 4M. Consequently, in the strongly accumulated regime carrier, scatterings due to electron-electron interaction are reinforced in the narrow and dense channel of 1M devices.

In the transfer curve, I_{DS} is larger at positive (solid lines) V_{DS} than negative (dotted lines) V_{DS} especially in the subthreshold regime. We have redrawn transfer curves at $V_{DS} = \pm 3$ V with the ratio $R_{\Delta I} = (I_{DS}(+3V) - I_{DS}(-3\,V))/I_{DS}(-3\,V)$ to compare V_{DS} polarity quantitatively in the inset of Fig. 1(f). Positive $R_{\Delta I}$ indicates higher I_{DS} at positive V_{DS}. Substantial distinction was mainly observed below zero V_{BG} with the largest $R_{\Delta I}$ of 130 in 4M-BG. Normalized output curves by $I_{DS}(+3\,V)$ manifest diode-like nonlinear behavior in the off regime and evolve into more symmetric (though still nonlinear) ones up to $V_{BG} = 20$ V as shown in Figs. 1(j)–1(l).

When applying positive (negative) V_{DS} on Ti contact, graphene (Ti) plays the role of source junction in n-type MoS_2 transistors. The overall observed data, such as diode-like behavior in normalized I_{DS}-V_{DS}, higher I_{DS} in positive V_{DS}, positive $R_{\Delta I}$, confirm the enhanced injection efficiency from the graphene contact rather than the Ti contact, particularly in the subthreshold regime. The increased van der Waals interaction and electron transfer from MoS_2 to graphene shown in Raman[10] are accountable for barrier lowering and hence injection efficiency in our fabricated devices.

We extracted device parameters from transfer curves: cut-off voltage (V_{OFF}), threshold voltage (V_{TH}), subthreshold swing (SS), and field-effect mobility (μ_{FE}). V_{OFF}, the gate voltage where channel surface potential crosses Fermi level (E_F) of MoS_2, is obtained from the V_{BG} of minimum current and shown in Fig. 2(a). V_{OFF} decreases with V_{DS} magnitude but no distinction can be drawn with V_{DS} polarity (positive V_{DS} shown in closed circles and negative V_{DS} shown in open circles). V_{TH} shown in Fig. 2(b) also decreases with V_{DS} but in contrast to V_{OFF}, V_{TH} is lower at positive V_{DS} (closed circle) indicating polarity dependence. V_{DS} dependent parameter variation in Fig. 2 is ascribed to non-ohmic SB behavior.

V_{DS} dependence of V_{TH} in our transistor is not consistent with the results in conventional transistors. If the second order term of V_{DS}, which is generally neglected, is included in channel current, V_{TH} should increase as a function of V_{DS} as shown in following equation. $I_{DS}(V_{GS}) = L/W\mu_{FE}C_{OX}$ $[(V_{GS} - V_{TH})V_{DS} - V_{DS}^2/2] = L/W\mu_{FE}C_{OX}[V_{GS} - (V_{TH} + V_{DS}/2)V_{DS}]$, where C_{OX} and V_{GS} are gate oxide capacitance and gate-source voltage, respectively.[13] We should note here that the lowest V_{OFF} was observed in 4M-BG, while the lowest V_{TH} was observed in 4M-SG.

Fig. 2(c) plots SS ($dV_{GS}/d(\log I_{DS})$) which is the gate voltage required to increase channel current by a decade in

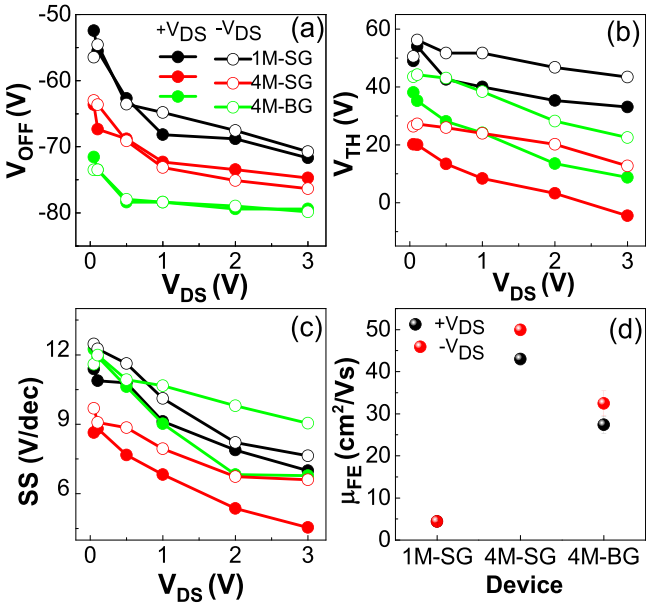

FIG. 2. V_{DS} dependent (a) V_{OFF}, (b) threshold voltage (V_{TH}) extracted by conventional linear extrapolation method, (c) Subthreshold swing (SS), and (d) field-effect mobility (μ_{FE}).

the subthreshold regime. SS variation results from the serially connected capacitance to C_{OX}.[13] With negligible interface states, the contribution by depletion capacitance in channel or metal-channel overlapped area should explain the V_{DS} dependence of SS variation. In Fig. 2(d), the field effect mobility is calculated by the equation $\mu_{FE} = g_{max}L(WC_{OX}V_{DS})^{-1}$.[3] A g_{max} represents the maximum of transconductance $\partial I_{DS}/\partial V_{GS}$ and is obtained around $V_{BG} = 60$–80 V. The extracted μ_{FE} at positive (negative) V_{DS} in 1M-SG, 4M-SG, and 4M-BG correspond to 4.4 ± 0.33 (4.4 ± 1.1), 42.9 ± 1.5 (49.9 ± 0.6), and 27.4 ± 2.1 (32.5 ± 2.9) cm^2/V s, respectively.

To analyze the details of 4M-SG and 4M-BG transistors, the previous transfer curves were replotted in Fig. 3(a) for fixed $V_{DS} = 0.1$ V, 1 V, and 3 V. 4M-SG demonstrated higher V_{OFF} and lower V_{TH} than 4M-BG implying improved gate

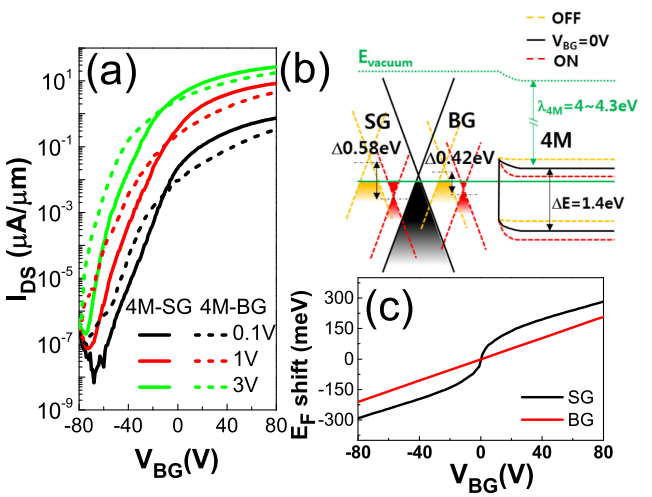

FIG. 3. (a) Transfer curves of 4M-SG (lines) and 4M-BG (dotted lines) at $V_{DS} = 0.1$ V (black), 1 V (red), and 3 V (green).(b) The comparison of band diagram for 4M-SG and 4M-BG. (c) Calculated E_F variation of SG and BG by gate voltage.

control due to the SB modulation of graphene-MoS_2 junction during transitioning from complete depletion to flat band of the surface channel.

The band diagram for gate modulation was illustrated in Fig. 3(b). Negative V_{BG} down-shifts E_F by p-doping graphene, while positive V_{BG} up-shifts E_F by n-doping graphene. Respective up- and down-shifts of graphene E_F with n-type MoS_2 induce the increase and the decrease in SB height. The E_F variation of SG and BG can be described by the change of carrier density (n) induced by gate voltage, i.e., $E_F = \hbar v_F(\pi n)^{1/2}$ for SG and $E_F = \pi\hbar^2/2m^*$ for BG, where $v_F = 1 \times 10^6$ m/s is the Fermi velocity of SG, and $m^* = 0.033m_e$ is the effective mass of carrier in BG relative to the bare electron mass m_e.[9] This was also observed by work function measurement, which showed an excellent agreement.[14] With 300 nm SiO_2 gate oxide, the range of E_F shift corresponds to $\sim\pm200$ meV and $\sim\pm300$ meV with $V_{BG} = \pm80$ V for SG and BG, respectively, as shown in Fig. 3(c). Therefore, in 4M-SG devices, I_{OFF} is suppressed by larger SB height, while I_{ON} is conversely enhanced by lower SB height

As we noted in Fig. 2, the lower V_{OFF} in 4M-BG along with the lower V_{TH} in 4M-SG makes it obvious that SS and μ_{FE} are also enhanced in 4M-SG. During transistor operation, higher on/off ratio of 4M-SG originates from both lower I_{OFF} and higher I_{ON}.

We extracted differential conductance (σ_d) from I_{DS}-V_{DS} at constant V_{BG} by differentiating I_{DS} with respect to V_{DS} as shown in Fig. 4. The σ_d curves reveal several distinct features not easily observed from the I_{DS}-V_{DS} curves. First, highly asymmetric curves of σ_d become more symmetric with increased V_{BG}. This is from the relatively reduced effect of asymmetric SB at high gate bias. Second, σ_d increased 6 orders for 1M-SG, while it increased only 3 orders in 4M devices as V_{BG} increased from -60 V to 80 V. Third, for 4M devices σ_d in 4M-BG than 4M-SG starts off higher at $V_{BG} = -60$ V, however, the trend reverses and σ_d of 4M-BG is lower at $V_{BG} = 0$ V, and the ratio of σ_d for 4M-SG to 4M-BG remains approximately 1.5 above $V_{BG} = 20$ V.

σ_d includes terms from channel and contact contributions. Since the channel material is equivalently 4M, the contact contribution determines σ_d evolution as a function of V_{DS}. Recalling earlier that μ_{FE} of 4M-SG was 1.5 times that of 4M-BG, similar to the σ_d ratios between 4M-SG to 4M-BG. Our results show some evidence that the mobility enhancement of 4M-SG may be connected to improved contact resistance in the accumulation regime. Both I_{DS}-V_{BG} and σ_d establish that SG might be favorable as an electrode, demonstrating raised on/off ratio, improved SS, and μ_{FE} than BG.

The saturation of σ_d and eventual decrease were observed at positive V_{DS} in the accumulation regime of both 4M-SG and 4M-BG as shown in Fig. 4 from $V_{BG} = 20$ V to 80 V, but not for 1M devices. As previously mentioned, if σ_d changes are related with contact resistance, then the ohmic-like 4M-graphene junction can explain this behavior. In fact, at $V_{BG} > 20$ V pulling the conduction band close to E_F in n-type MoS_2 considerably drops SB width, which allows for efficient carrier injection by tunneling through a transparent SB of nearly negligible width. However, the eventual saturation level of σ_d is lower than that of the 4M-Ti junction which shows monotonic growth at negative V_{DS}. High graphene sheet resistance could be a major culprit in limiting

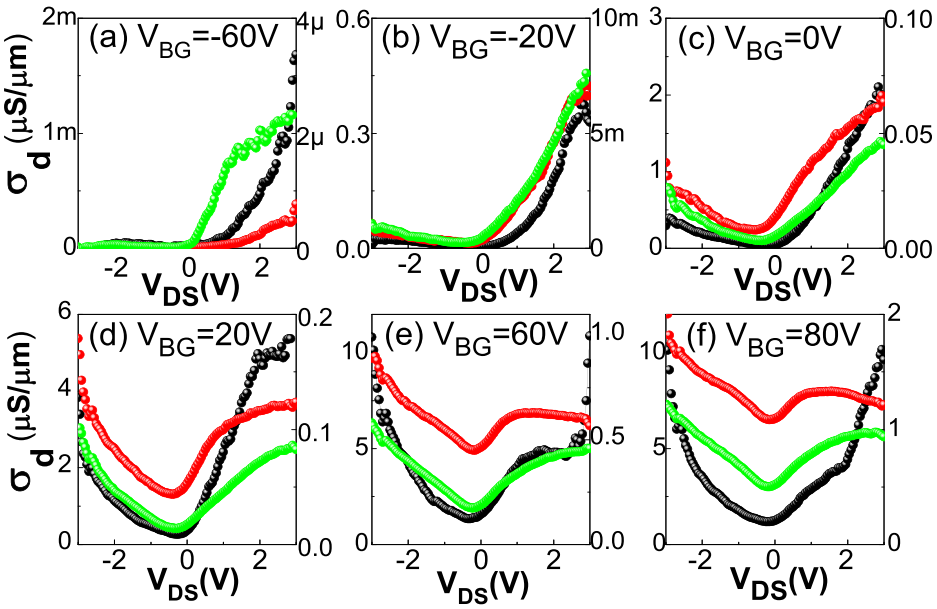

FIG. 4. V_{DS} dependent differential conductance (σ_d) of 1M-SG (black), 4M-SG (red), and 4M-BG (green). Left-axis scale for 4M-SG and 4M-BG and right-axis scale for 1M-SG.

conductance.[15] In contrast to the improved performance in the subthreshold regime, μ_{FE} decline in graphene source electrode devices seems to be associated with limited σ_d at a rather low saturation level. From the point of view of applications, when high concentrations of charge carriers must be delivered, we can speculate that graphene could be a poor choice of source electrode.

In conclusion, transport properties on metal-MoS_2-graphene transistors revealed enhanced performance with graphene as source electrode particularly in the subthreshold regime. On the contrary, μ_{FE} measurement showed the opposite results. V_{DS} polarity dependence of device parameters, such as SS and V_{TH}, was ascribed to the asymmetric Schottky barrier height. We confirmed that single-layer graphene as source electrode provides improved transistor properties than that of bi-layer as demonstrated with lower SS and larger μ_{FE}. However, in spite of improved charge carrier injection, graphene can still be unfavorable in the strongly accumulated regime if employed for high current delivery without further improved sheet resistance.

This research was supported by Basic Science Research Program through the National Research Foundation of Korea (NRF) (Grant No. 2013R1A1A3007993).

[1]S. Das, H.-Y. Chen, A. V. Penumatcha, and J. Appenzeller, Nano Lett. **13**, 100 (2013).
[2]H. S. Lee, S. S. Baik, K. Lee, S.-W. Min, P. J. Jeon, J. S. Kim, K. Choi, H. J. Choi, J. H. Kim, and S. Im, ACS Nano **9**, 8312 (2015).
[3]B. Radisavljevic, A. Radenovic, J. Brivio, V. Giacometti, and A. Kis, Nat. Nanotechnol. **6**, 147 (2011).
[4]W. S. Leong, X. Luo, Y. Li, K. H. Khoo, S. Y. Quek, and J. T. L. Thong, ACS Nano **9**, 869 (2015).
[5]C. Gong, C. Huang, J. Miller, L. Cheng, Y. Hao, D. Cobden, J. Kim, R. S. Ruoff, R. M. Wallace, K. Cho, X. Xu, and Y. J. Chabal, ACS Nano **7**, 11350 (2013).
[6]R. Moriya, T. Yamaguchi, Y. Inoue, S. Morikawa, Y. Sata, S. Masubuchi, and T. Machida, Appl. Phys. Lett. **105**, 083119 (2014).
[7]Y. T. Lee, K. Choi, H. S. Lee, S.-W. Min, P. J. Jeon, D. K. Hwang, H. J. Choi, and S. Im, Small **10**, 2356 (2014).
[8]J. Yoon, W. Park, G.-Y. Bae, Y. Kim, H. S. Jang, Y. Hyun, S. K. Lim, Y. H. Kahng, W.-K. Hong, B. H. Lee, and H. C. Ko, Small **9**, 3295 (2013).
[9]S. Das Sarma, S. Adam, E. H. Hwang, and E. Rossi, Rev. Mod. Phys. **83**, 407 (2011).
[10]See supplementary material at http://dx.doi.org/10.1063/1.4937266 for the followings: Schematic illustration of fabrication process; thickness analyzation of 2D materials by AFM and Raman; Raman spectra of MoS2 and MoS2/graphene overlapped area; and photocurrent mapping image VBG = 0 V.
[11]R. Schlaf, O. Lang, C. Pettenkofer, and W. Jaegermann, J. Appl. Phys. **85**, 2732 (1999).
[12]J. Y. Kwak, J. Hwang, B. Calderon, H. Alsalman, N. Munoz, B. Schutter, and M. G. Spencer, Nano Lett. **14**, 4511 (2014).
[13]B. G. Streetman, *Solid State Electronic Devices*, 6th ed. (Prentice Hall, 2005).
[14]Y.-J. Yu, Y. Zhao, S. Ryu, L. E. Brus, K. S. Kim, and P. Kim, Nano Lett. **9**, 3430 (2009).
[15]F. Xia, V. Perebeinos, Y.-m. Lin, Y. Wu, and P. Avouris, Nat Nanotechnol. **6**, 179 (2011).